




# Generalized data-driven optimal path planning framework for uniform coverage missions using crop spraying UAVs

Rohit V. Nanavati<sup>1</sup> · Yanhua Meng<sup>2</sup> · Matthew Coombes<sup>1</sup>  · Cunjia Liu<sup>1</sup>

Accepted: 19 February 2023 / Published online: 16 March 2023  
© The Author(s) 2023

## Abstract

Unmanned aerial vehicle (UAV) based crop spraying has become a popular alternative in the field of precision agriculture. One of the key goals of UAV based spraying is achieving spray coverage that is as uniform as possible to ensure maximum spray efficacy. Most of the existing studies in the literature focus on analysing the effects of spraying parameters on the uniformity of coverage distribution using experimental studies. However, in this work, we propose a novel generalized data-driven optimal path-planning framework aimed at finding the optimal operational flight parameters (flight speed and pass widths) for a lawnmower coverage path plan to meet the specified spray coverage rate while ensuring the uniformity. The framework takes a spray distribution model as an input and computes the optimal operational parameters for the coverage path plan to minimize coverage non-uniformity without making any assumptions on the UAV type. Furthermore, we also propose a neural network structure using Gaussian kernel neurons to design the spraying model using experimental data. The neural network structure makes no assumption about the type of UAV, onboard nozzle placement, or the flight parameters. The accuracy of the modelling solution only depends on the quality of the training data. In other words, higher diversity of the training data in terms of the flight and spraying parameters would result in a modelling solution that is more representative of the spraying distribution and consequently improve the quality of the operational parameters obtained from the proposed optimization framework. In this work, we present a case study to demonstrate the use case and test the performance of the proposed framework via simulation and experiments using the DJI AGRAS-T10 drone. The results showed that the optimal pass-width solutions for low forward speeds were similar to optimizing the positioning of the nozzles on a boom sprayer to achieve uniform coverage. Whereas, at high speeds, the pass-width was comparatively higher as the spread of the effective coverage over each pass increased. A discussion contextualized in the case study is provided to highlight the salient features and limitations of the proposed framework.

**Keywords** UAV · Crop spraying · Uniform coverage · Optimization · Coverage path planning

---

✉ Matthew Coombes  
m.j.coombes@lboro.ac.uk

Extended author information available on the last page of the article

## Introduction

Improvement in agricultural practices utilising the advancements in robotics has been a focus of research for the last two decades. Field survey, mapping and monitored crop protection from pests is critical in ensuring cultivation of healthy and safe agricultural produce (Mulla, 2013). The use of unmanned aerial vehicles (UAVs) to achieve these aforementioned objectives is being explored, especially in the area of smart aerial spraying as discussed in (Lan et al., 2017; Mogili & Deepak, 2018; Radoglou-Grammatikis et al., 2020; Tellaeche et al., 2008). The use of crop spraying UAVs for precision agriculture allows one to eliminate the health risks associated with manual spraying of pesticides, along with increasing the spray coverage in a limited span of time. In addition, they are able to spray areas inaccessible to humans and machinery. To ensure crop health, the task of spraying pesticides need to be carried out with high precision as over or under spraying may have detrimental effects on the crop health. To achieve this the spray needs to be applied uniformly at the correct application rate. This is made more complex as the spray distribution from a UAV unlike traditional tractor boom sprayers is highly non-uniform, as shown in Coombes et al. (2022). This warrants smart path planning for UAV based spraying missions. Such a path planning mission would consist of two key parts: (1) modelling of the spray distribution over a single pass for a UAV, followed by (2) solving for optimal UAV speed and waypoints to generate uniform coverage at the required application rate.

The spray distribution generated by an UAV depends non-linearly on a plethora of factors like temperature, nozzle features (Fornasiero et al., 2017), rotor angular speeds (Guo et al., 2021a, b), operational UAV speed and height (Qin et al., 2016), etc. The effects of different nozzle types on spray drift were discussed in (Fornasiero et al., 2017). Another study presented by (Wang et al., 2020) also discussed the spray drift properties of commercially available nozzles mounted on a four-rotor UAVs. Furthermore, the variation of spray distribution properties with respect to the type of pesticide and the temperature during spraying are considered in (Luo et al., 2017) for a task allocation problem between multiple UAVs. Due to large number of complex factors that govern spray distributions from a drone as discussed in the aforementioned works, analytically modelling the spray profile for is a non-trivial task. Furthermore, each drone would have a different spray distribution depending on its construction. This necessitates a modelling framework that can use a diverse set of experimental spray distribution data, obtained by varying different flight parameters, to map a specific spraying configuration to a modelling solution. Neural network-based modelling is one such potential modelling framework that can achieve the aforementioned task.

Neural network (NN) based modelling (LeCun et al., 2015) has been proven to capture the complex non-linear relationships between input–output datasets for applications pertaining to precision agriculture as discussed in studies like Kamilaris et al. (2017). Azizpanah et al. (2015) presented a neural network model to predict the sprayer drift properties under different weather conditions by processing water sensitive paper (WSP). The NN based algorithm proposed in Gao et al. (2019) was designed to identify areas to be sprayed by an UAV-based sprayer using 4 K images captured by the onboard computers. It is important to note that a *good quality* distribution modelling solution is necessary in generating a *good quality* path planning solution as the overall distribution over a field will be a superposition of coverage across multiple passes. For a neural network based modelling solution, a *good quality* model is usually quantified using the mean square error between the model and the experimental data. Zhang et al. (2018) developed an experimental spray

rig to simulate UAV spraying performance under different test conditions. Such platforms can be useful in obtaining the required experimental data necessary for training a neural network. However, for a small-scale application, experimental data for a specific UAV can be obtained via other techniques discussed in the literature. One such setup will be discussed in this work in later sections.

In the upcoming subsection, we discuss some related works that were designed with the objective of analysing achieved uniformity for a given UAV and spraying configurations and/or achieving a desired coverage distribution.

## Related work

In the literature, there are various studies that discuss the uniformity of coverage achieved by UAV based spraying. In studies like (Chen et al., 2021; Guo et al., 2021a, b; Meng et al., 2019, 2020; Wang et al., 2018), the effects of operational parameters on the coverage uniformity with the UAV flying in lawnmower path were discussed. The primary focus of these studies was to map the effect of the flight heights, speeds, droplet size, crop phenotype and spray volumes on the coverage distribution. However, the pass width and the UAV speeds were not chosen to optimise spray uniformity or application rate. Moreover, the achieved uniformity was evaluated using the coefficient of variations (CV) index (ratio of the standard deviation to the mean) which varied from 30 to 90% for UAV-based spraying. Another study presented in Shilin et al. (2017) studied the coverage uniformity performance across four different UAVs and also reported a CV ranging between 30 and 70%. The pass-width chosen in Shilin et al. (2017) did not consider an optimization constraints. On the contrary, the uniformity of spray distribution using boom-based spraying using ground vehicles is lower than 20% (Forney et al., 2017). This emphasizes the inherent inconsistent and non-uniform coverage achieved by drone-based spraying. The study presented in Forney et al. (2017) analysed the effects of nozzle positioning and orientation on boom-based spraying application. A typical boom-based spraying is carried using land vehicles at low speeds and low altitudes to ensure effective coverage and penetration. It was shown in Forney et al. (2017) that the uniformity of achieved coverage was higher on a boom structure when the nozzles were within 50 to 100 cm of each other. However, the effectiveness of a boom-based spraying operation is expected to degrade at higher speeds and warrants analysis especially when coupled with UAVs.

A desired coverage profile can be achieved either by controlling the nozzle flow rate and/or by controlling the operational parameters like UAV trajectory and its corresponding speeds. In (El Aissaoui, 2015), a feasibility study of direct injection spraying system was conducted that used variable application rate control with speed sensing information. A variable application rate solution usually needs some feedback data like speed and current coverage, etc., to compute the control action, resulting in a complex process control design solution which the commercially available agricultural drones are not generally equipped to handle. A lawnmower pattern is the most commonly used spraying path planning solution used to cover the area of interest for spraying applications in agricultural (Guo et al., 2021a, b) and paint deposition in automotive industries (Conner et al., 2005). This is because it tends to be the most time efficient path for concave regions (Choset, 2000), as well as being highly ordered making it easier and safer for operators. In Guo et al., 2021a, b, a model fitting method was used to capture the dependency of rotor speed and the achieved spray coverage in an laboratory setting, followed by an pass-width optimization solution that aimed at achieving a variable coverage distribution with constant flow

rate spraying. The path planning solution proposed by Guo et al., (2021a, b) optimized for pass-width and UAV speed along a lawnmower pattern. However, the performance of the scheme proposed in Guo et al., (2021a, b) was only tested in numerical simulation and did not capture the effects of UAV forward speed on the achieved coverage distribution. In the light of the discussion presented so far, in this paper, we will be focusing on obtaining an optimal path planning solution for UAV based spraying application where the UAV is following a lawnmower path. The contributions of the proposed work will be discussed in the next subsection.

## Contributions and organization

The primary contribution of this paper is proposing a novel generalized data-driven modelling and optimal path planning framework for a UAV based crop spraying application. This framework consists of two components: (a) A radial-basis function based neural network design has been presented with the objective of modelling the spray distribution of a UAV over a single pass; (b) Using the neural network modelling solution, an optimization framework is developed that solves for the optimal pass-width by penalizing the slope profile between consecutive passes to increase coverage uniformity, and the optimal speed by minimizing the error between the mean coverage and the desired coverage using the optimal pass-width solution.

The implementability and performance of the proposed framework has been studied using a case study with simulation and experimental evaluation performed for the DJI AGRAS-T10 agricultural drone. The case study using the AGRAS T10 UAV involved training the neural network using experimental spray coverage data obtained at different speeds and fixed height, followed by using the obtained modelling solution to evaluate the performance of the proposed scheme to achieve a desired uniform coverage. The training data was restricted to a fixed fly height to primarily focus on the correlation between the achieved coverage and UAV speed; however, the proposed modelling framework is not restricted to such flight conditions, rather the proposed neural network-based modelling framework is equally applicable to diverse set of training data obtained by varying flight and spray parameters like flight height, flow rate, nozzle placement, etc. It is worthy to note that the neural network based modelling solution proposed in this paper is flexible in modelling spray distribution behaviour of different UAVs in contrast to the model fitting based modelling solution presented in (Y. Guo et al., 2021a, b). Furthermore, the features of the proposed scheme along with the experimental performance is discussed in relation to the quality of modelling solutions obtained from the neural network.

The remainder of the paper is organized as follows: "[Problem formulation](#)" section formally defines the problem statement, followed by the coverage modelling solutions in "[Spray distribution modelling](#)" section. The "[Spray distribution modelling](#)" section discusses the spray distribution modelling using a neural network. "[Path planning](#)" section contains the design and derivation of the optimal pass-width and UAV speed solutions. "[Case study—numerical and experimental study](#)" section presents a case study that analyses the implementability and use case for the proposed modelling and optimization framework. "[Case study—numerical and experimental study](#)" section consist of five subsections that discuss the methods of obtaining and analysing training data, obtaining the optimal flight operational parameters, and, a simulation and experimental study analysing the resulting overall coverage using on the obtained

modelling and optimal operational flight parameters obtained in the previous subsections. Finally, “Conclusion” section concludes the paper by providing a summary of the key results.

## Problem formulation

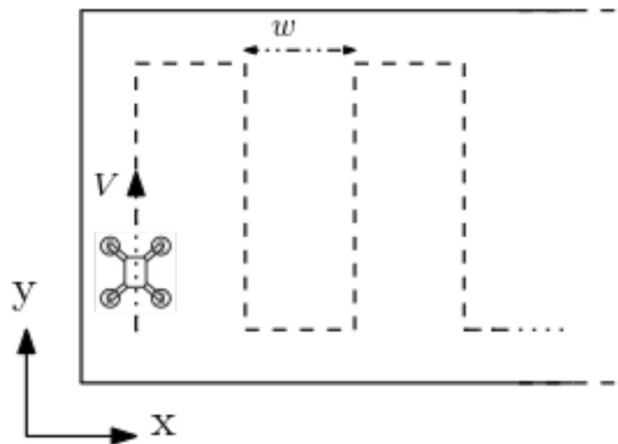
In this section, we formally define the path planning problem to achieve a desired uniform coverage profile over a predefined region of interest using an unmanned aerial vehicle. The UAV is assumed to be following a lawnmower pattern to cover the area of interest. The lawnmower pattern is a conventional spraying strategy with parallel linear longitudinal paths results in a pattern as shown in Fig. 1. Let the desired percentage coverage at any given point  $(x, y) \in \mathcal{S}$  in physical space be denoted by  $D(x, y)$ , where  $\mathcal{S}$  denotes the set of all points of interest. The design goals of the path planning problem for UAV based crop spraying are twofold: (a) obtain a model that captures the spray distribution perpendicular to the flight direction for a given set of spraying parameters like flight height, spray volume, nozzle features, etc., and (b) Utilize the developed spray distribution model to generate the set of UAV waypoints and their speeds such that the deviation of the resultant coverage distribution is minimized. Let an element of such a set be denoted by  $(x^*, y^*, V^*)$ .

For a given spraying configuration (fixed flow rate), the relationship between the lateral coverage distribution and the UAV speed can be modelled as inversely proportional, as discussed in Coombes et al., 2022. In other words, a faster moving UAV would result in lower coverage as compared to a slowly moving UAV. Such an explicit inverse dependency between the UAV speed and the lateral coverage distribution, albeit not ideal, is a reasonable assumption which will be demonstrated to hold using experimental data later in the paper. Therefore, the overall coverage distribution,  $d$ , at any position  $(x, y)$  can be modelled as

$$d(x, y) \propto \frac{1}{V(x, y)} \Rightarrow d(x, y)V(x, y) = \text{constant} = \Phi(x, y)$$

where the UAV speed at  $(x, y)$  is denoted by  $V$  and the proportionality constant represents analogue to the application rate conservation of spraying agent under a fixed flow rate. Suppose the spray distribution in the lateral direction, along the  $x$  axis, generated by an UAV moving in the longitudinal direction, along the  $y$  axis, at a speed of 1 m/s is denoted

**Fig. 1** Schematic drawing of the lawnmower path followed by the UAV



by  $\Phi(x, y)$ . Therefore, from the above expression, the proportionality constant is equal to  $\Phi(x, y)$  and has the units  $\%Area^{\frac{m}{s}}$ . Moreover, the achieved spray distribution  $d(x, y)$  at a UAV speed  $V$  has the units of  $\%Area$ . Therefore, using a modelling solution for  $\Phi(x, y)$ , one can compute the coverage distribution  $d(x, y)$  at some UAV speed.

To ensure a uniform coverage distribution, an objective function designed to penalize the error between the achieved and desired coverage along the lateral direction is chosen. It should be noted that, for a uniform desired deposition profile, the speed solution across each path of the lawnmower pattern remains the same along with the width between consecutive passes. This simplifies the design objective to obtaining the spray distribution model along with the best UAV speed,  $V$ , and pass-width,  $w$ , required to minimize the non-uniformity of the achieved coverage. The optimization objective can be written as

$$\min_{(w^*, V^*)} J = \int_S [d(x, y, V) - D(x, y)]^2 dx dy \tag{1}$$

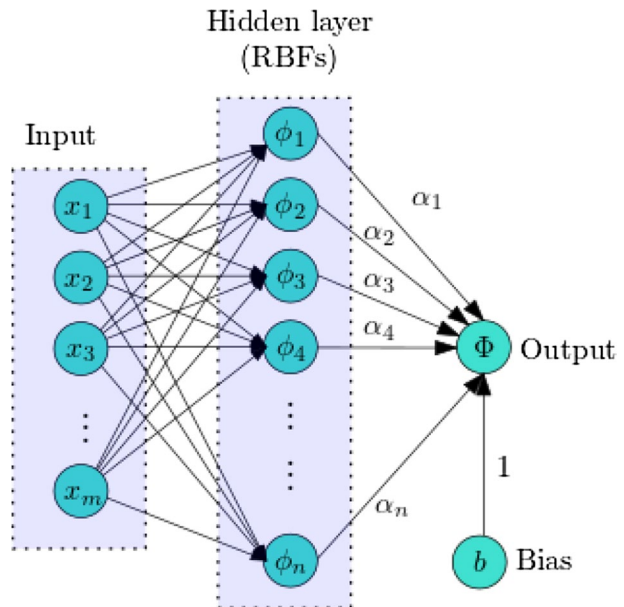
where  $D(x, y) := M$  is the desired constant coverage to be achieved by the UAV and  $w^*$  is the optimal pass-width solution.

### Spray distribution modelling

In this section, we employ a neural network-based framework to address the first design goal of the path planning problem, namely modelling the lateral spray distribution of the UAV over a single pass for a given spraying configuration.

In this paper, we employ a network structure with Gaussian kernel functions, also referred to as radial basis function in the literature. The neural network is structured as a three-layer NN model, with an input, hidden and output layer as shown in Fig. 2. The input layer consists of the input vectors which are used to generate centre vectors of the

**Fig. 2** Architecture of radial basis function network: The input layer consist of the training data points with each data point can consist of flight and spray parameters. The hidden layer consists of neurons modelled as radial basis function, whose hyperparameters are chosen based on unsupervised learning from the data points of the input layer. Finally, the output modelled solution is a linear weighted combination of the neurons of the hidden layer along with an additional bias



radial basis functions using unsupervised learning. The centre vectors serve as the mean value of the multivariate Gaussian kernels. The hidden layer consists of the radial basis functions usually referred to as neurons. The output is a scalar function represented as the weighted sum of the RBFs along with a modelling bias as shown in Fig. 2. For the application at hand, we focus on modelling the distribution function  $\Phi$  and the lateral distance  $x$  perpendicular to the direction of UAV path, where the modelling parameters capture the effect of aerodynamic and UAV factors like nozzle type, fly height, flow rate, etc.

Let the radial basis functions,  $\phi_j$ , be mathematically represented as

$$\phi_j = \exp\left[-\beta^2(x - \mu_j)^2\right] \quad \forall j = 1, 2, \dots, n \quad (2)$$

where  $n$  is the number of neurons in the hidden layer,  $\mu_j$  are the centres,  $\beta$  is the spread of a Gaussian kernel, and  $x$  is the lateral distance from a reference. The spread  $\beta$  is a specified parameter, however, the kernel centres are learned from the input layer using unsupervised learning.

From the network structure in Fig. 2, the resulting spray distribution,  $\Phi(x)$ , can be expressed as

$$\Phi(x) = b + \sum_1^n \alpha_j \exp\left[-\beta^2(x - \mu_j)^2\right] \quad (3)$$

where  $\alpha_j$  are weights signifying the contribution of each kernel in the output and  $b$  is a bias vector corresponding to the output layer. The coefficients  $\alpha_j$  and  $b$  are obtained by minimizing the mean square error (MSE) between the experimental output  $\hat{\Phi}$  and the modelling distribution i.e.,  $|\hat{\Phi} - \Phi(x)|^2$  summed over all the training data. The number of neurons  $n$  in the hidden layer can be iteratively increased to ensure that the MSE of the modelled solution and the experimental data converges below an acceptable threshold.

**Remark 1** Note that for the proposed modelling design, the input layer consists only of lateral distance  $x$  establishing its explicit dependency with respect to  $\Phi$ . However, the dependence of spraying and aerodynamic parameters to  $\Phi$  is implicit. For an explicit dependency between the spraying and aerodynamic parameters, the input layer can be modified to account these parametric variations. For example, one can capture the variation across flight heights and flow rates by choosing the neuron structure as follows.

$$\bar{\Phi}(x) = b + \sum_1^n \alpha_j \exp\left[-\beta^2(x - \mu_{xj})^2 - \beta^2(h - \mu_{hj})^2 - \beta^2(f_r - \mu_{fj})^2\right]$$

where  $x$ ,  $h$ , and  $f_r$  denote the lateral distance, flight height, and flow rate, respectively, along with  $\mu_{xj}$ ,  $\mu_{hj}$  and  $\mu_{fj}$  denoting the kernel centres of the neural network with respect to the lateral distance, height, and flow rate. Such a model that captures explicit variation across all such flight and spraying parameters would require an extensively diverse training data set to effectively model the spray distribution. However, obtaining experimental data for a diverse training parameter set can be complicated. Therefore, in this work to make experimentally obtaining training data feasible, we focus on only modelling the explicit dependence between  $\Phi$  and  $x$  for a given spraying configuration using Eq. (3), and we leave the study of a modelling solution  $\bar{\Phi}(x)$  for future research. In practice, one could also employ computational fluid dynamics-based techniques to obtain extensive training data at diverse flight configurations.

### Path planning

In this section, we design a path planning solution to achieve uniform coverage distribution by generating the optimal pass-width solution along with the corresponding optimal pass speed solution for a lawnmower path traced by the UAV. To obtain the optimal pass-width and speed solution, we make the following assumptions:

**Assumption 1** The spray distribution curve,  $\Phi$  remains fixed throughout the entire application, that is, the flow rate from each UAV nozzle is maintained at a constant value.

**Assumption 2** The operational altitude of the UAV is maintained at a fixed value over the entire application profile.

**Assumption 3** The pass-width between the  $i + 1^{th}$  and  $i^{th}$  pass depend on the UAV spray distributions from the  $i - 1^{th}$ ,  $i^{th}$ ,  $i + 1^{th}$  and  $i + 2^{th}$  passes.

Let the spray distribution curve corresponding to the  $i^{th}$  curve be denoted by  $\Phi_i$ . Moreover, let the lateral position to the centre of  $\Phi_i$  be denoted by  $\bar{\mu}_i$  as shown in Fig. 3.

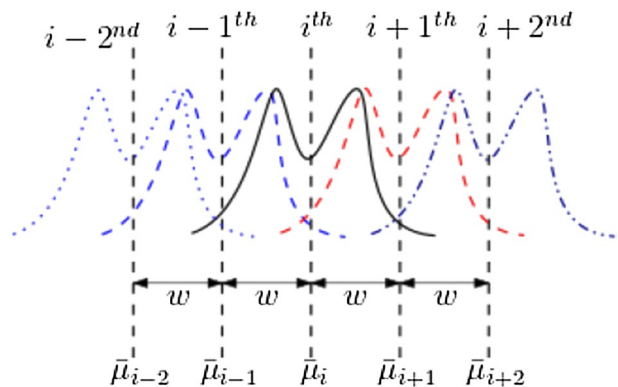
The pass-width is now formally defined as the distance between the centre of consecutive passes, that is,  $\bar{\mu}_{i+1}$  and  $\bar{\mu}_i$ . In other words,  $\bar{\mu}_{i+1} = \bar{\mu}_i + w$ . Moreover, under Assumption 1, the spray distribution profile corresponding to the  $i + 1^{th}$  pass can be expressed using the modelling solution from the previous section as  $\Phi_{i+1} = \Phi(x + iw)$ , where  $\Phi(x)$  is the modelling solution. Let the overall coverage distribution achieved over  $k$  passes be denoted by  $\tilde{\Phi} = \Phi_1 + \Phi_2 + \dots + \Phi_k$ . Let the error between overall coverage distribution and the desired coverage be defined as

$$e = \frac{\tilde{\Phi}(k,w)}{V} - M \tag{4}$$

with  $kw$  as the lateral dimension of the field of interest. The optimal solution for UAV speed,  $V^*$ , pass-width,  $w^*$ , and the number of passes satisfies the relation  $kw^* =$  width of the field of interest, can be obtained by solving the following optimization problem

$$(V^*, w^*) = \operatorname{argmin}_{w,V} \int_{S(k)} e^2(w, V) dx$$

**Fig. 3** Superposition of spray distributions across different passes: This figure demonstrates Assumption 3 which implies that the coverage distribution between  $\bar{\mu}_i$  and  $\bar{\mu}_{i+1}$  depends on the spray distribution from the passes from the  $i - 1^{th}$ ,  $i^{th}$ ,  $i + 1^{th}$  and  $i + 2^{th}$  passes





However, on deriving the conditions of optimality, one can note that the resulting optimality conditions are coupled in nature, that is, the optimal pass-width and speed solutions are dependent on each other. This renders obtaining an analytical expression to optimal solution a non-trivial task. Therefore, in this paper, we focus on proposing a framework to decouple the aforementioned optimization problem into two sub-problems to obtain the optimal pass-width and the corresponding optimal UAV speed solution to achieve a resulting coverage as close to a desired coverage.

### Pass-width optimization

To avoid a coupled optimization problem, we define an alternative optimization index aimed to solve for the optimal pass-width,  $w_{min}$ , as follows

$$\min_{w \in (0, 2\epsilon]} J_a = \frac{1}{kw} \int_0^{kw} \left[ \frac{d\tilde{\Phi}}{dx} \right]^2 dx \tag{5}$$

where  $\epsilon$  is the upper limit on the feasible pass-width for the modelled distribution. For practical purposes, the upper limit  $\epsilon$  can be chosen based on the effective lateral coverage width over a single pass for a given spraying configuration. The objective function is designed to obtain a favourable pass-width solution by penalizing the variance of distribution slope profile from zero, where a slope profile equal to zero represents a uniform distribution. It is worthy to note that the proposed objective function is designed around the rate of change of the distribution profile in contrast to the actual coverage distribution for paint spraying applications as explored in Conner et al., (2005).

Under the Assumptions 1–3, the optimization can be focused on the variance between two consecutive passes, for brevity consider the 2nd and 3rd pass, simplifying  $J_a$  as

$$\min_{w \in (0, 2f)} J_a = \frac{1}{w} \int_{\bar{\mu}_i + 2w}^{\bar{\mu}_i + 3w} \left[ \frac{d\tilde{\Phi}}{dx} \right]^2 dx \tag{6}$$

where  $\tilde{\Phi}$  for  $x \in [\bar{\mu}_i + 2w, \bar{\mu}_i + 3w]$  can be approximated, using the aforementioned assumptions, as

$$\tilde{\Phi}(x) \approx \Phi_1 + \Phi_2 + \Phi_3 + \Phi_4 \approx 4b + \sum_{i=1}^{i=4} \sum_{j=1}^{j=n} \alpha_j e^{[-\beta^2(x - \mu_j - iw + w)^2]} \tag{7}$$

Using Eq. (3), the derivative of  $\tilde{\Phi}$  can be obtained as

$$\begin{aligned} \frac{d\tilde{\Phi}}{dx} &= \frac{d}{dx} [\Phi_1 + \Phi_2 + \Phi_3 + \Phi_4] \\ &= \sum_{i=1}^{i=4} \sum_{j=1}^{j=n} \left\{ -2\alpha_j \beta^2 (x - \mu_j - iw + w) e^{[-\beta^2(x - \mu_j - iw + w)^2]} \right\} \end{aligned} \tag{8}$$

The optimal pass width,  $w^*$ , that minimizes the objective function Eq. (6) can be chosen using line search optimization techniques in the literature or gradient-descent techniques using the gradient obtained in Eq. (8). So far, we obtained a pass-width solution that ensured a close to uniform profile based on slope variations, however, no constraints on the mean coverage distribution were imposed. For agricultural applications, a desired spray

coverage is needed to effectively achieve the spraying objective. In the next subsection, we pose an optimization problem to choose the optimal UAV speed solution using the optimal pass width solution obtained by minimizing Eq. (6).

### Speed optimization

In this subsection, we focus on obtaining the optimal speed for each pass of the UAV for the pass-width solution  $w^*$  with  $\Phi$  being the spray distribution modelling solution obtained from the neural network. The chosen optimization index is expressed as

$$\min V J_v = \int_{\bar{\mu}_1+2w_{min}}^{\bar{\mu}_1+3w_{min}} \left[ \frac{\tilde{\Phi}}{V} - M \right]^2 dx \tag{9}$$

The objective function  $J_v$  is designed to minimize the variation of the resultant coverage profile from the desired coverage distribution, in other words, driving the mean of the resultant coverage profile to  $M$ . Differentiating  $J_v$  with respect to  $V$ , one may obtain

$$\frac{dJ_v}{dV} = \int_{\bar{\mu}_1+2w_{min}}^{\bar{\mu}_1+3w_{min}} 2 \left[ \frac{\tilde{\Phi}}{V} - M \right] \left[ \frac{-\tilde{\Phi}}{V^2} \right] dx \tag{10}$$

The slope  $dJ_v/dV$  is equal to zero when the integrand of Eq. (10) is zero. Therefore, by equating the integrand to zero, one can express the optimal UAV speed as

$$V^* = \left[ \int_{\bar{\mu}_1+2w_{min}}^{\bar{\mu}_1+3w_{min}} \tilde{\Phi}^2 dx \right] \left[ M \int_{\bar{\mu}_1+2w_{min}}^{\bar{\mu}_1+3w_{min}} \tilde{\Phi} dx \right]^{-1} \tag{11}$$

The optimal UAV speed given by Eq. (11) ensures that variance of the achieved coverage distribution  $\tilde{\Phi}/V$  across the desired coverage of  $M$  is minimized. In the next section, we analyse the performance of the data driven optimization framework discussed so far.

## Case study—numerical and experimental study

In this section, we study the performance of the proposed path planning algorithm using simulation and experimental studies for multiple desired percentage coverage. Firstly, we discuss the experimental procedure, setup and materials needed to gather the experimental data used for training the neural network. Note, that as discussed in Remark 1, we focus on modelling the explicit dependency of the spray distribution  $\Phi$  and  $x$  for a fixed set of flight and spray parameters. The case study discussed in this section is a representative example of a use case of the proposed framework and similar studies can be conducted for different flight configurations, drone types, etc., as the no assumptions on the drone type or flight configurations are made in the design of the proposed framework.

### Training data gathering for spray distribution modelling

In this subsection, we aim to gather experimental data relating the coverage variation in the lateral direction  $d$  for a given spraying configuration. The UAV used for the presented



**Fig. 4** Agras T10 drone by DJI

**Table 1** DJI Agras T10 drone specs

| Classification                                  | Parameters                   |
|---|------------------------------|
| Dimensions with extended arms and blades        | 1 958 mm × 1,833 mm × 553 mm |
| Dimensions with extended arms and blades folded | 1 232 mm × 1 112 mm × 553 mm |
| Operation tank volume                           | 8 L at full load             |
| Number of sprayers                              | 4 (Nozzle model: XR11001VS)  |
| Water pump model                                | Diaphragm pump               |
| Positioning mode                                | GPS + GLONASS                |
| Load capacity                                   | 8 L                          |

research is the DJI Agras T10 drone (Fig. 4: Agras T10 drone by DJI). The technical parameters for the UAV are given in Table 1.

The experimental setup to obtain lateral coverage measurements is shown in Figs. 5, 6. We use water sensitive paper (WSPs, 26 × 76 mm) as an artificial sampler to gather the percentage coverage data for the drone spraying water. The entire setup can be divided into three regions namely—left, central and right zones. The central zone refers to the WSPs labelled  $c_6$  to  $c_{12}$ , where WSPs  $c_6 \rightarrow c_8$  and  $c_{10} \rightarrow c_{12}$  have a spacing of 20 cm and WSPs  $c_9 \rightarrow c_{10}$  have a spacing of 10 cm. Therefore, the central zone is approximately 1.0 m wide and corresponds to the region that falls directly below the span of the drone (which is equal to around 1.232 m). The left and right zone, as the name suggest, lie to the left and right of the drone trajectory, respectively, with the objective of measuring the spraying coverage away from the drone on either side. The spacing between the WSPs in the left and right zones is 30 cm resulting in an overall width of these zones as approximately 1.5 m each. The setup has three rows separated by 15 m and containing 17 WSP strips each positioned as shown in Fig. 3. The sampling width of 4 m is chosen as at least thrice the span of the spraying drone, AGRAS-T10, which is approximately 1.23 m. It is assumed that a majority of the spray particulates would be captured within a sampling width of 4 m. It should be noted that for a different flight configuration or larger drone, the sampling width can be extended appropriately such that the drone span is below fifty percent of the entire sampling width.

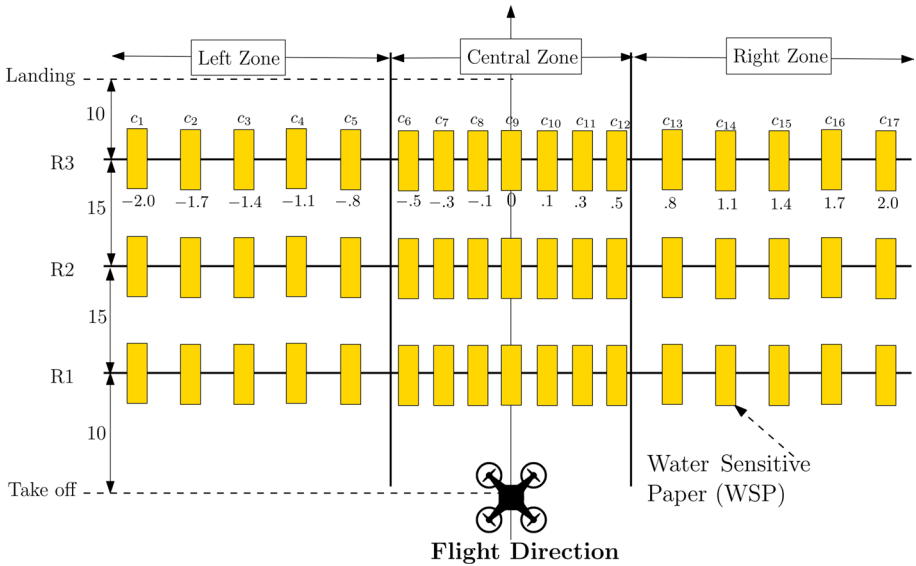


**Fig. 5** Schematic of the Experimental Setup: The experimental setup proposed here is to measure the spray distribution resulting from UAV based spraying. The yellow rectangles represent a water sensitive paper strip used for measuring the coverage achieved at each sampling point. The central zone has higher density of water sensitive paper to obtain more training data points directly below the drone



**Fig. 6** Experimental Setup at a football field, where researchers can be seen collecting WSP samples after a spray run

The density of WSPs in the central zone is chosen to be higher as compared to that of the left (and right) zones to capture any spray overlap from the nozzles on either side of the drone. The UAV is flown autonomously at a set speed and height as measured by RTK GNSS and a radar altimeter respectively, flying straight down the middle of the central zone. The UAV is commanded to start spraying 10 m before the first row to ensure that the WSPs are exposed to a steady state spray flow through the nozzles.

We design the single swath data for the different configurations as mentioned in Table 2. The total flow rate was chosen to be 1.2 L/min for all flight configurations.

**Table 2** Experimental flight parameters for data collection to be used for training the neural network designed in the previous section

| Configuration | Flight height (m) | UAV speed (m/s) |
|---------------|-------------------|-----------------|
| C1            | 1.5               | 1               |
| C2            | 1.5               | 2               |
| C3            | 2.0               | 3               |
| C4            | 2.0               | 3.5             |
| C5            | 2.0               | 4               |

All the data collection experiments were conducted such that the UAV is flying upwind. The data collection was conducted early morning between 6 and 8am on the 21st of June 2022 as the ambient wind speeds were in a desirable range of 0–2 m/s. Furthermore, the average temperature on the day was 12.5 °C. The data collection was conducted in a level football field located at 52.75702°N and – 1.24276°E. The nearby tree line was at least 30 m away from the experimental setup.

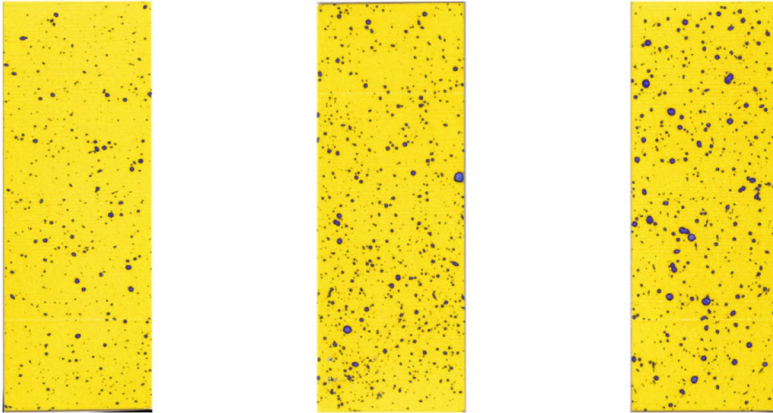
**Remark 2** The water-sensitive paper-based method to measure the coverage distribution can be very resource intensive and complex especially when one wishes to obtain a extensively diverse set of data for training of the neural network. An alternative to this method can be computational fluid dynamics-based simulation platforms that enable the used to artificially generate distribution measurements with higher resolution and for various flight configurations.

## Analysis of training data and modelling

Similar to the image-based analysis tool used in Ahmad et al. (2020), the software ImageJ was used to analyse the collected water sensitive papers using a 1200 DPI coloured scanner in the presented work. The ImageJ software was used to compute the overall area covered by water, mean diameter of droplets, and percentage area exposed to water. The coverage of a WSP is same as the percentage area exposed to water. Figure 7 shows a few examples of the WSPs collected after the spray run.

**Remark 3** It is worthy to note that using the coverage information along with mean diameter measurements corresponding to each droplet, one can compute the application rate or volume sprayed per unit area. However, the involved computations are not accurate in our opinion and therefore, the percentage coverage has been chosen as the preferred index for path planning optimization.

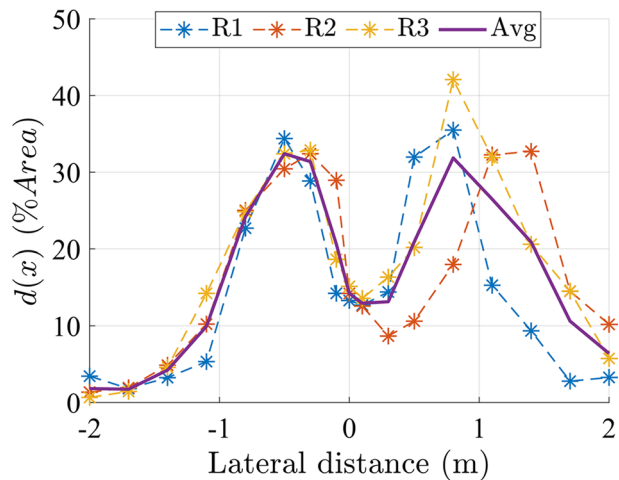
The spray distribution from experimental runs mentioned in Table 2 are plotted in Figs. 8, 9, 10, 11, 12. Additionally, an average percentage coverage across three rows has also been plotted along with the experimental data. It can be seen from Figs. 8, 9, 10, 11, 12 that the resulting spray distribution has two peaks which roughly align with the nozzle placement on the drone. Furthermore, it can also be seen that as the UAV speed increases, the magnitude of the achieved coverage decreases inversely. The mean coverage across the 17 sampling locations for configuration C1 to C5 were 16.7,



(a) Coverage of 3.29 %. (b) Coverage of 6.24 %. (c) Coverage of 6.63 %.

**Fig. 7** Example of water sensitive paper collected after a spray run. These water sensitive paper correspond to the first row of the flight run corresponding to configuration 3 and belong to the central zone, namely  $c_4$ ,  $c_5$  and  $c_6$ , respectively, as per the schematic shown in Fig. 3

**Fig. 8** Spray distribution for C1 config



7.4, 4.7, 4.1 and 3.4%, respectively. This inverse dependency between the coverage and speed would be used for modelling the spray distribution of a UAV in the upcoming section.

**Remark 4** It is worthy to note that the bimodal nature of the spray distribution may result in an infeasible pass-width solution or a non-uniform coverage distribution over multiple pass. However, the proposed framework in the upcoming sections is designed to compute the best possible optimal operational point for the available spray distribution. A more uniform spray distribution for a different drone and spraying configurations may result in a more uniform coverage distribution.

**Fig. 9** Spray distribution for C2 config

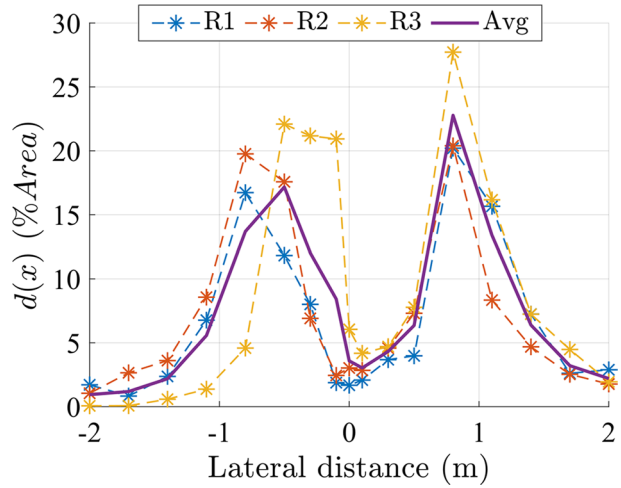
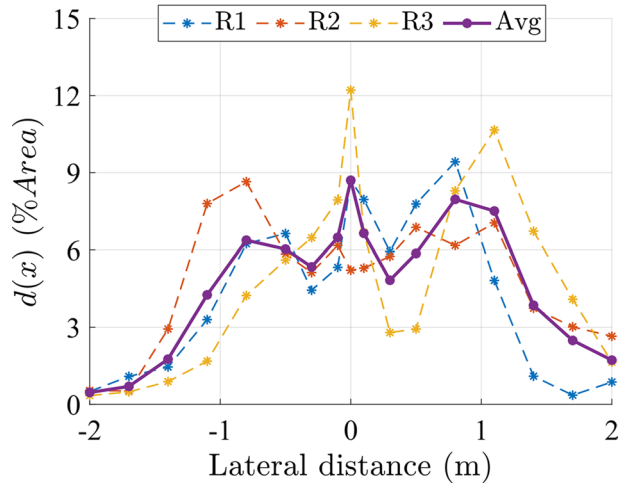


**Fig. 10** Spray distribution for C3 config



We now use the obtained experimental data to train the RBF based neural network. Note that the experimental data is the effective coverage  $d(x)$ , however, the neural network is designed to model the proportionality constant i.e., the spray distribution at UAV speed of 1 m/s,  $\Phi(x)$ . Therefore, the training data can be obtained by multiplying the experimental data with the flight speeds as per the relationship  $\hat{\Phi}(x) = d(x) \times V$ .

The spray distribution for higher speed flights differs to low-speed flights due to the aerodynamic interaction between the spray particles and the downwash from the UAV rotors. Therefore, the obtained experimental data is now classified into two sets. The data obtained for configuration C1 and C2 are used to generate a modelling solution corresponding to low-speed and low altitude flights, whereas configuration C3 to C5 are used to generate a modelling solution corresponding to the high-speed high-altitude flights. To create and train the RBF-NN, we use the *newrb* function in MATLAB that adds a specified width Gaussian neuron one-by-one to iteratively reduce the mean-square error below the goal MSE.

**Fig. 11** Spray distribution for C4 config

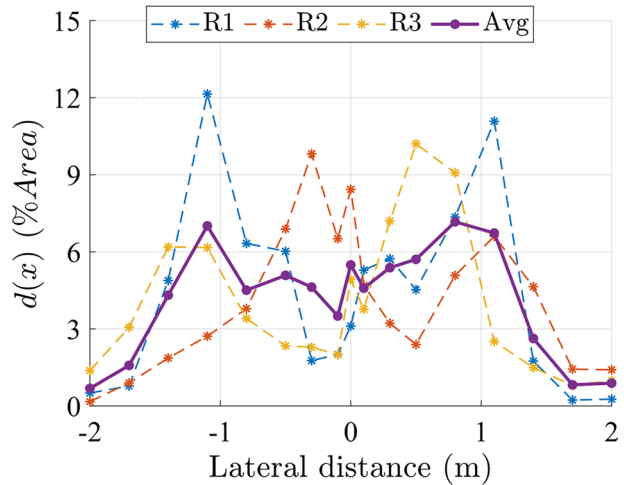
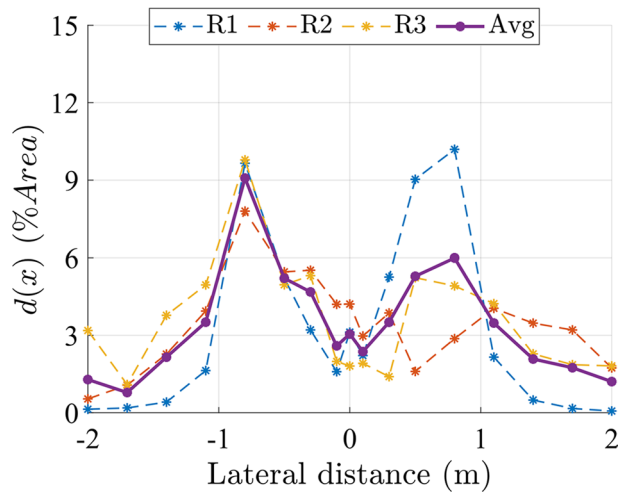


**Fig. 12** Spray distribution for C5 config



The resultant RBF-NN model for the spray distribution corresponding to low-speed low altitude flights are presented in Fig. 13. Whereas the modelling solution to configuration C3–C5 are plotted in Fig. 14. It can be seen from Fig. 13 that the resulting modelling solution for low-speed flights has a bimodal nature with the location of these peaks roughly aligning with the nozzle placements on the UAV. The coverage difference between the peaks and valley for low-speed flights was approximately 30%. Furthermore, similar bimodal behaviour was obtained for high-speed flights as seen from Fig. 14. However, the coverage difference between the peaks and valley for high-speed flights was approximately 8%, which is significantly lower than the low-speed flight solution. Moreover, the modelling solution corresponding to high-speed flights has a larger spread compared to the low-speed modelling solution. The error bars presented in Figs. 13, 14 represent the standard deviation of the modelling solution from the experimental data at each sampling location. It can be seen from the aforementioned figures that the resulting models have a significant standard deviation around



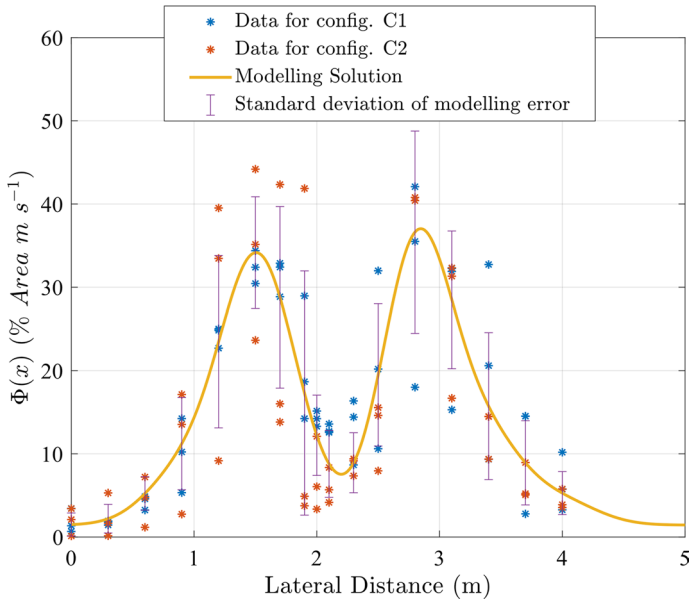


Fig. 13 Modelling output from trained neural network corresponding to config. C1 and C2

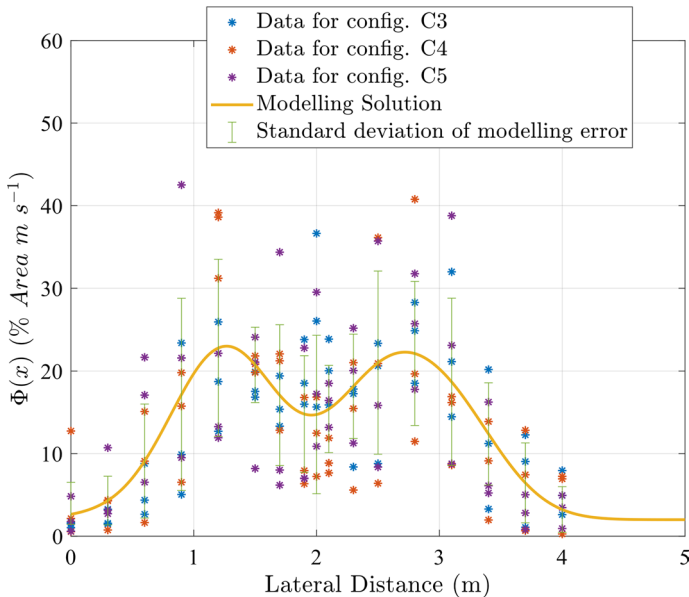


Fig. 14 Modelling output from trained neural network corresponding to config. C3, C4 and C5

the peaks. One of the key reasons behind such a significant standard deviation is the inherent inconsistency associated with spraying using a UAV primarily caused due to the interaction between the spray particles and the downwash as well as variability in the

wind. These modelling errors can be further minimized by choosing a different kernel function for the neural network; however, this would induce design complexities in obtaining a path planning solution. The choice of an RBF kernel was primarily motivated by the structural features of the experimental data along with the ease a Gaussian kernel provides in classifying and generating a path planning solution.

**Remark 5** It is worthy to note that the proposed neural network does not assume the UAV type, nozzle properties or the flow rate settings. The proposed network can be used to generate a modelling solution using the obtained experimental data. In other words, behaviour of the distribution due to variation in flow rate, flight height and other spraying parameters can be captured by simply training the network on the relevant experimental data obtained at the desired flight conditions. For the proposed study, the experimental data was obtained for a fixed height, nozzle type, flow rate settings for the AGRAS T10 agricultural drone.

In the upcoming subsection, we use both the modelling solutions presented in Figs. 13, 14 to obtain the corresponding optimal path planning solutions and analyse its dependency on the features of each modelling solution like peaks and valleys in modelled spray distribution.

### Optimal pass-width and UAV speed solution

Using the RBF-NN model solutions generated in the previous subsection, the dependency of  $J_a$  with respect to the pass-width can be studied from Figs. 15 and 16 for the low-speed and high-speed modelling solutions, respectively. The upper limit  $\epsilon$  is chosen at the distance between the nozzles of the AGRAS-T10. Therefore, for the simulation study,  $\epsilon$  is chosen to be 1.225 m. Hence, the optimal solution of the pass-width belongs to  $w \in [0, 2.5]$ .

It can be noted from Fig. 15 that the optimizing index corresponding to the low-speed modelling solution is non-monotonic in nature, that is, there exist multiple pass-width solution that correspond to a local minimum. The two peaks near a pass-width of 0.5 m and 1.4 m corresponding to the scenario where the bimodal distribution across a pass-width causes a constructive interference resulting in increase of non-uniformity in the overall distribution. The

**Fig. 15**  $J_a$  Vs. pass-width for the low-speed modelling solution

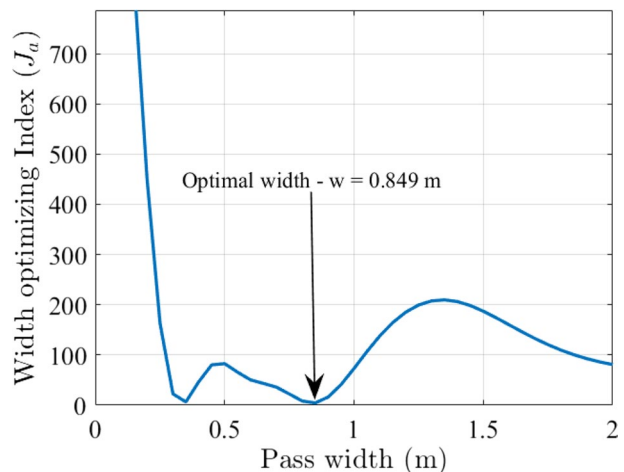
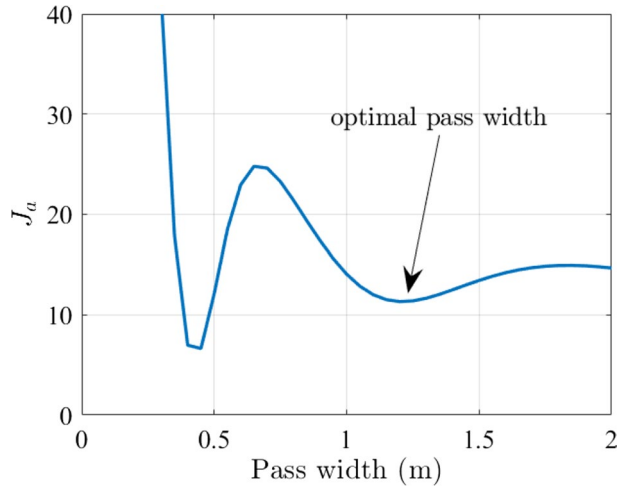


**Fig. 16**  $J_a$  Vs. pass-width for the high-speed modelling solution



optimal solution can be found by using a line-search method like the golden-section technique. Moreover, it can also be noted that the local minima corresponding to a pass-width of 0.35 m would demand higher number of passes to cover the area of interest, which is undesirable. Hence, the pass-width solution of 0.35 m is discarded, and the width of 0.85 m is chosen as the optimal solution. As discussed in the Introduction section, for crops like wheat, rice and corn, a uniform coverage distribution is ideal and boom sprayers are the most popular spraying techniques used for such crops. The resultant lawnmower path flown by the UAV with an optimal pass-width of 0.85 m is a close analogue of the behaviour of a boom spraying mechanism, where the spray nozzles are placed closer to each other to obtain a uniform spraying profile and the forward movement of the boom is usually slow. For a boom spraying setup, it was shown in Forney et al. (2017) that the overall coverage profile is more uniform for smaller nozzle placement distance.

From Fig. 16, it can be noted that the optimizing index corresponding to the high-speed modelling solution presented a similar non-monotonic nature to the previous case. However, the resulting optimal pass-width solution corresponding to the high-speed modelling solution was approximately 1.35 m. The increase in the optimal pass-width solution can be attributed to the relative larger spread of the high-speed modelling solution as compared to the low-speed modelling solution. Furthermore, a pass-width solution of 1.35 m would allow a UAV to cover larger areas quickly in contrast to the pass-width solution of 0.85 m. This emphasizes the advantage of investigating and analysing the performance of the high-speed modelling solution in a practical setting. For the remainder of the paper, we restrict our analysis and testing to the high-speed modelling solution. Table 3 contains the UAV speed for different desired coverage distribution computed using Eq. (11) for a pass-width of 1.35 m corresponding to the high-speed modelling solution. It is worthy to note that the optimal UAV speed is dependent

**Table 3** Optimal UAV speed for different desired percentage coverage at  $w^* = 1.35m$

| Desired coverage (%) | Optimal speed (m/s) |
|----------------------|---------------------|
| 15                   | 4.11                |
| 20                   | 3.05                |

**Fig. 17** Coverage distribution using the proposed algorithm,  $d(x, y)$  for  $M=15\%$  obtained using a pass-width of 1.35 m, UAV speed of 4.11 m/s and a flight height of 2 m

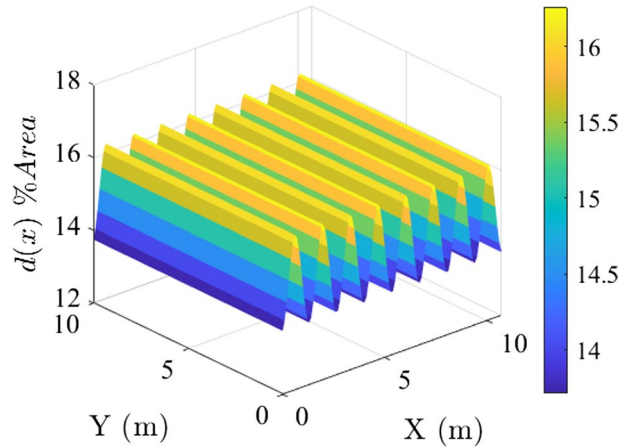
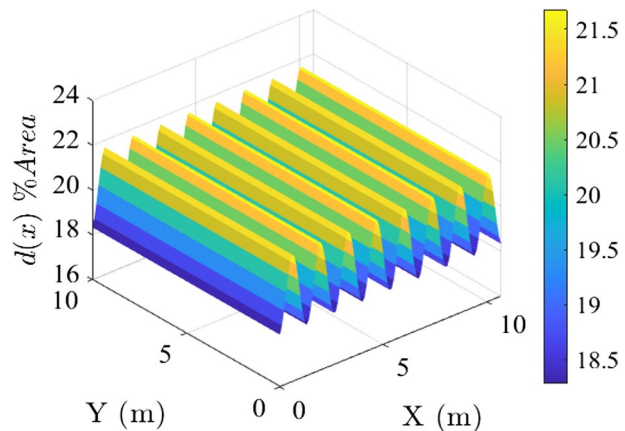


**Fig. 18** Coverage distribution using the proposed algorithm,  $d(x, y)$  for  $M=20\%$  obtained as per a pass-width of 1.35 m, UAV speed of 3.05 m/s and a flight height of 2 m



on the choice of pass-width solution. Table 3 contains the optimal UAV speed corresponding to the optimal pass-width of 1.35 m for different desired percentage coverage.

## Simulation study

For simulation studies, consider an area of interest of dimensions  $10m \times 10m$ . The spraying parameters are chosen same as mentioned in Table 1. Additionally, for the simulation study, the flight height for the UAV is assumed to be same as the fly height used for the modelling data, that is, 2 m. Furthermore, in order to eliminate the edge effect and avoid negating Assumption 3, two additional passes are considered before and after the desired spray area is covered. The pass-width is chosen to be 1.35 m as per the discussion in the previous sections. Therefore, the overall number of passes along the  $x$  direction is  $k = \lceil 10/1.3 \rceil + 4 = 12$ . Moreover, the performance of the proposed algorithm is presented by plotting the achieved coverage distribution  $d(x, y)$  for multiple desired coverage distribution at the optimal operation parameters. The UAV speed is computed as per the discussion in the previous sections.

**Fig. 19** Coverage distribution using the proposed algorithm,  $d(x, y)$  using a pass-width of 1 m, UAV speed of 3.05 m/s and a flight height of 2 m

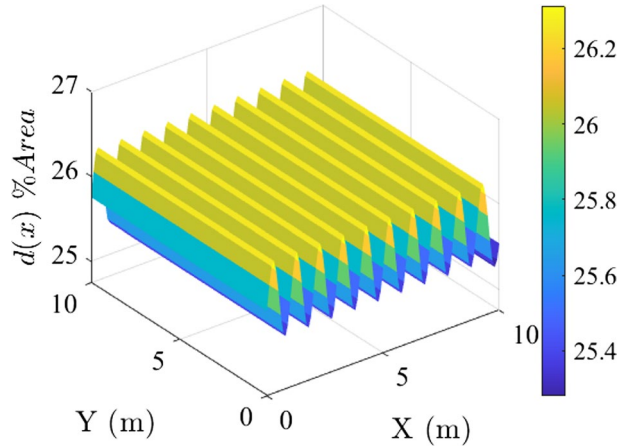
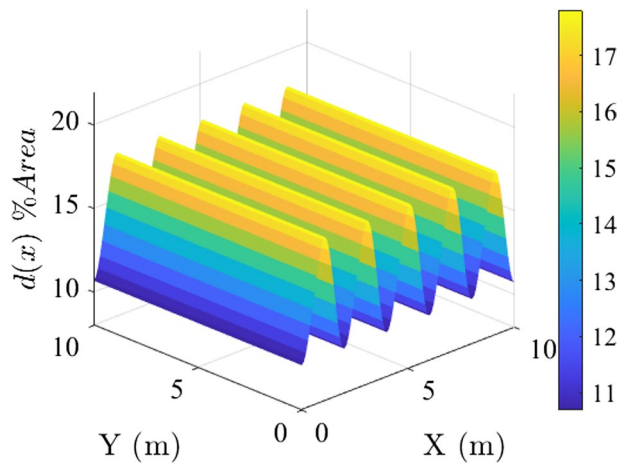


**Fig. 20** Coverage distribution using the proposed algorithm,  $d(x, y)$  using a pass-width of 2 m, UAV speed of 3.05 m/s and a flight height of 2 m



The simulation results presented in Figs. Figures 17 and 18 correspond to the case with a uniform desired coverage along the  $10m \times 10m$  field of interest. The Figs. Figures 17 and 18 corresponding to the achieved coverage distribution for a desired mean coverage of 15% and 20%, respectively, with the operational parameters chosen as per the discussion in the previous subsections.

Additionally, we also present simulation results for different combinations of pass-width and UAV speed combination to emphasise the optimality of the optimal combination discussed in the previous subsections. Recall that the goal of achieving a desired mean coverage of 20%, the optimal pass-width and UAV speed combination based on the discussion so far is  $(w^*, V^*) = (1.35, 3.05)$ . Therefore, we now present the achieved coverage using a set of pass-width and UAV speed combinations that vary around the aforementioned optimal combination. Consider the following pass-width and UAV speed combinations:  $(w(m), V(m/s)) = (1, 3.05), (2, 3.05), (1.35, 2.5), \text{ and } (1.35, 5)$ . We will now demonstrate that the variations across the optimal combination results either in higher non-uniformity or larger error in mean achieved coverage. The simulation results corresponding to the

**Fig. 21** Coverage distribution using the proposed algorithm,  $d(x, y)$  using a pass-width of 1.35 m, UAV speed of 2.5 m/s and a flight height of 2 m

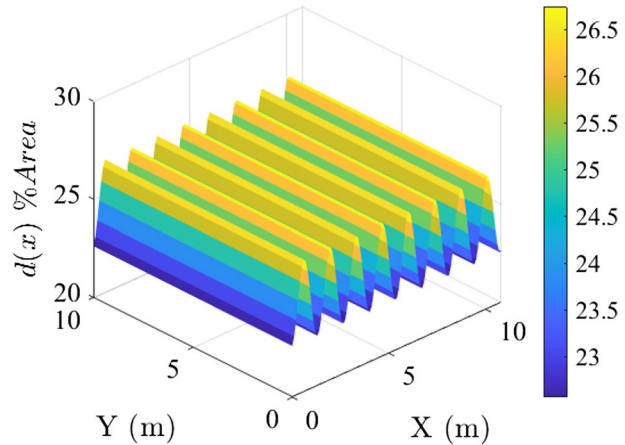
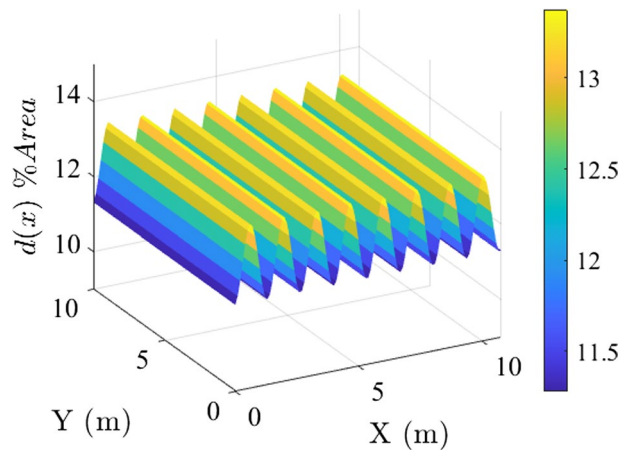


**Fig. 22** Coverage distribution using the proposed algorithm,  $d(x, y)$  using a pass-width of 1.35 m, UAV speed of 5 m/s and a flight height of 2 m



above-mentioned pass-width and UAV speed combinations are provided in Figs. 19, 20, 21 and 22, respectively.

It can be seen from Fig. 19 that if the pass-width is chosen lower than the optimal value of 1.35 m, the achieved mean coverage corresponding to  $(w, V) = (1, 3.05)$  resulted mean coverage is approximately 6% higher than the desired value of 20%. Similarly, for a pass-width larger than  $(w, V) = (2, 3.05)$ , it can be seen from the Fig. 20 the resulting achieved mean coverage distribution is approximately 5% lower than the desired coverage of 20% along with variation of 7% between the peak and value of the resulting distribution. Furthermore, the achieved coverage distribution for variations in UAV speed is presented in Figs. 21 and 22. Similar, to the previous discussion, the achieved mean coverage distribution for a faster and slower choice of UAV speed (5 m/s and 2.5 m/s, respectively) resulted in significant error in the achieved mean coverage distribution.

Moreover, for the optimal combination of  $(w^*, V^*) = (1.35, 3.05)$ , it can be seen from Figs. 17 and 18 that the error in coverage distribution corresponding the optimal configuration is  $e = |d(x, y) - M| \leq 1.5\%$  for both  $M = 15\%$  and  $20\%$ . This demonstrates the accuracy and effectiveness of the proposed framework to achieve a desired coverage percentage

in a simulation environment. Moreover, it can be seen that the maximum error between the achieved and the desired coverage is positively correlated to the magnitude of the desired coverage distribution. One potential reasoning behind this correlation is the bimodal nature of the modelling solution. At lower speeds (higher mean coverage), the peaks across consecutive passes are constructively superimposed resulting in larger variations away from the desired coverage.

In the subsequent subsection, we conduct an experimental study to analyse the performance of the proposed algorithm against uniform desired coverage across the field of interest.

## Experimental study

In the previous subsection, we discussed a framework to obtain an optimal UAV speed and pass-width solution to minimize the variance of the achieved coverage from a desired value, given some modelling data for a UAV.

However, no system constraints were considered in obtaining the aforementioned optimal solutions. Most of the commercially available agricultural UAVs may have inherent systems constraints on speed and pass-widths to ensure safe operational conditions. Therefore, analysing the optimal solutions while considering the system constraints becomes important subjective to the available UAV. The agricultural UAV, AGRAS-T10, used in this study limits the achievable pass-width between 1.6 and 3 m along with a maximum operational speed of 7 m/s.

Therefore, the experimental study is conducted at a pass-width solution of 1.6 m which would increase the non-uniformity of the achieved coverage as discussed in the "[Pass-width optimization](#)" section. Furthermore, the AGRAS-T10 is flown in autonomous mode at a height of 2 m from the WSP using its onboard software once the required flight height, forward speed, pass-width, and area of interest information is selected using its controller. The experimental study was conducted at the same football field where the data collection for modelling was done. The experimental study was conducted on 23rd June 2022 between 6 and 8am with a mean ambient temperature of approximately 13 °C and mean wind speed of approximately 2.5 m/s.

It is important to note that the operational constraints are subjective to the UAV used which may or may not allow for optimal operational conditions. Furthermore, the UAV speed, computed using Eq. (11), for a pass width of 1.6 m corresponding to 15% and 20% desired coverage are presented in Table 4. The UAV flight height is chosen to be 2 m from the water sensitive paper.

The setup for the experimental study is shown in Fig. 23. The setup consists of two rows separated by 10 m each consisting of 21 pieces of water sensitive paper placed at a distance of 30 cm apart. Similar to the simulation study, the UAV flight plan consist of two additional passes before and after the edge of the rows. Two sets of experimental data have been collected for a desired distributions of 15% along with an additional set of data corresponding to

**Table 4** UAV speed for different desired percentage coverage at  $w = 1.6m$

| Desired Coverage (%) | Optimal speed (m/s) |
|----------------------|---------------------|
| 15                   | 3.50                |
| 20                   | 2.65                |

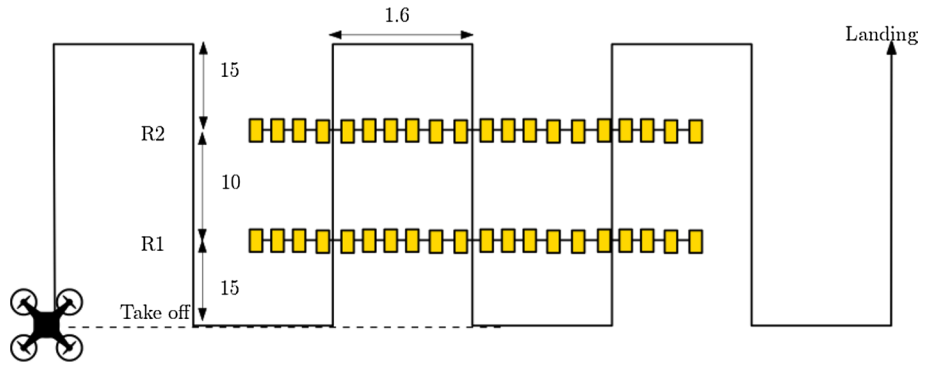


**Fig. 23** Experimental setup for testing the uniformity of the achieved coverage distribution over multiple passes

a desired coverage of 20%. The objective is to evaluate the uniformity of the achieved coverage using a measure called coefficient of variation.

The coefficient of variation (CV) for a set of  $M$  measurements denoted by  $X_1, X_2, \dots, X_S$  is defined as

$$CV(\%) = 100 \times \frac{\sigma}{\nu}, \quad \sigma = \sqrt{\frac{\sum_1^S (X_s - \nu)^2}{S-1}}$$

where  $\sigma$  and  $\nu$  are the standard deviation and mean of the data. A lower  $\sigma$  corresponds to higher uniformity of the data. Therefore, lower the CV the more uniform is the coverage

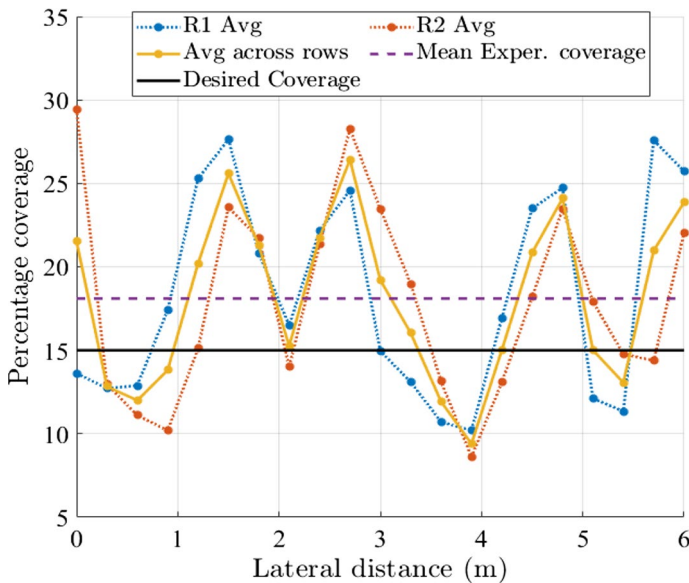


**Fig. 24** Coverage distribution at a UAV speed  $V=3.50$  m/s and a pass-width of 1.6 m



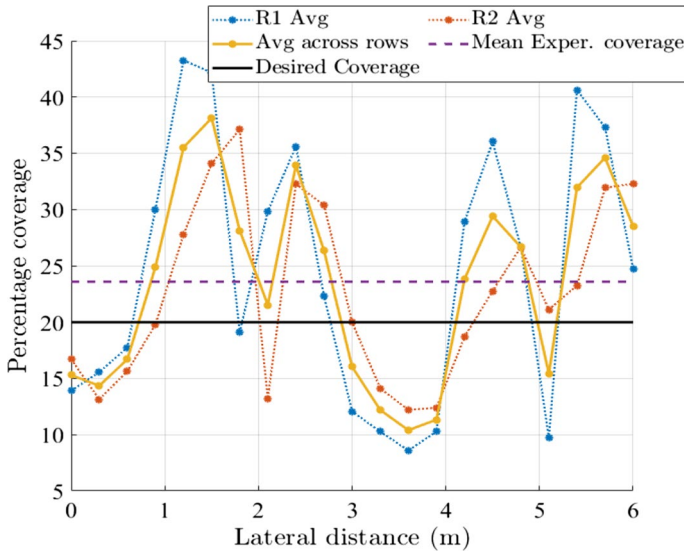


Fig. 25 Coverage distribution at a UAV speed  $V=2.65$  m/s and a pass-width of 1.6 m

Table 5 Experimental mean, standard deviations, and CVs across rows

|            | $\nu$ | $\sigma_{exp}$ | $\sigma_d$ | $CV_{exp}(\%)$ | $CV_d(\%)$ |
|------------|-------|----------------|------------|----------------|------------|
| $M = 15\%$ | 18.10 | 5.03           | 5.94       | 27.7           | 39.65      |
| $M = 20\%$ | 23.58 | 8.75           | 9.49       | 37.1           | 47.45      |

distribution. It has been shown in the literature that the CV achieved using a boom spraying structure tends to be below 20%, whereas UAV based spraying tends to be larger than 20%.

The experimental results corresponding to the desired coverage distribution of 15% are presented in Fig. 24. Figure 24 contains coverage distribution for Row 1 and 2, and an average for both, as well as the mean percentage coverage averaged over both rows shown as a dotted line. Furthermore, the achieved coverage is plotted using a dashed line. It can be seen that the experimental mean is 3.1% higher than the desired coverage of 15%. Similarly, the experimental coverage distribution for a desired coverage of 20% is plotted in Fig. 25. Similar to the previous case, the mean of the achieved average coverage is 3.5% higher than the desired value of 20%.

Let  $\nu$ ,  $\sigma_{exp}$ , and  $CV_{exp}$  denote the mean coverage achieved, the corresponding standard deviation and CV values obtained from the average coverage distribution across rows. Furthermore, let  $\sigma_d$  and  $CV_d$  denote the standard deviation and CV values across the desired coverage ( $M$ ) computed as

$$CV_d(\%) = 100 \times \frac{\sigma_d}{M}, \quad \sigma_d = \sqrt{\frac{\sum_{z=1}^{z=Z} (X_z - M)^2}{Z - 1}}$$

where  $X_z$  is the row-average coverage at  $z^{th}$  sampling location.

Note that while  $\sigma_{exp}$  and  $CV_{exp}$  provide a measure of uniformity of the row-averaged experimental data. Moreover, the metrics  $\sigma_d$  and  $CV_d$  provides a measure of uniformity across the desired coverage. Hence,  $\sigma_d$  and  $CV_d$  are useful in evaluating the performance of the proposed framework.

It can be noted from Table 5 that an  $CV_{exp}$  value of approximately 28% and 37% were achieved corresponding to the desired coverage of 15% and 20%, respectively, for a suboptimal pass width of 1.6 m imposed due to operational constraints. It should be noted that the achieved CV is expected to be further reduced under optimal conditions as discussed in the previous sections. Based on existing studies (Chen et al., 2021; Shilin et al., 2017) in the literature, the average achieved CV across different UAVs and/or spraying parameters ranged from 30 to 90% with a pass-width chosen without any uniformity optimization conditions. This emphasizes the advantage and usefulness of the proposed framework to further decrease the CV achieved from a spraying application which would consequently improve uniformity of the achieved coverage.

Furthermore, it can be noted that the  $CV_d$  values are higher in comparison to the  $CV_{exp}$  values. As the  $CV_d$  is computed with respect to the desired coverage,  $CV_d$  is higher than  $CV_{exp}$  due to the error in achieving the desired coverage. One of the key reasons for the error in achieved mean coverage can be attributed to the modelling errors incurred by the modelling solutions as shown in Fig. 14 and discussed in the previous subsections. Due to the inherent inconsistency of the modelling data obtained from an UAV flight, achieving a modelling solution that minimizes the modelling error becomes a non-trivial task. Therefore, such modelling errors are propagated through the optimization framework and possibly result in the error in achieving the desired mean coverage. One potential solution to improve the modelling solution to explore different nozzle placements along with UAV parameters. For example, a boom-like nozzle placement structure and a unirotor UAV, like the HyB-15L UAV as shown in Qin et al. (2016), can improve the overall spread of the achieved coverage, avoid multi-peak distribution and increase the effective swath achieved by an UAV in a single pass.

## Conclusion

In this paper, we proposed a novel data-driven generalized optimal path planning framework designed to solve for the optimal speed and pass-width for a UAV spraying application following a lawnmower pattern. The novelty of proposed framework is its ability to provide optimal operational flight parameters irrespective to the UAV type in contrast to the existing studies. In this study, the applicability of the proposed scheme was demonstrated for the DJI AGRAS-T10 UAV. We first obtain experimental single-pass spray distribution data for the UAV, which was used to train a radial-basis function based neural network. The neural network was designed to model the spray distribution of the UAV over a single pass and the resulting modelling solutions for the AGRAS-T10 were bimodal in nature. The distribution models were fed into an optimization framework designed to minimize the non-uniformity of the achieved coverage over multiple passes. The effects of the modelling solution on the optimal solution were discussed followed by a simulation study demonstrating coverage profile achieved using the derived model and optimization solution. Finally, an experimental study was conducted to analyse the effectiveness of the proposed framework. It was shown that the achieved CV index was considerably lower than the mean CV achieved by various UAVs in the existing studies that do not enforce any

optimization constraints. It should be noted that the proposed framework is also applicable for spray distribution data obtained in terms of application rate instead of percentage coverage. The percentage coverage was chosen to measure the spray distribution due to the ease and accuracy of measuring it from a water sensitive paper.

An interesting direction of future research would be to modify the neural network modelling to incorporate the effects of other flight parameters and nozzle placements, so that the proposed optimization framework can be applied to a wider range of spraying tasks. Moreover, a optimization framework that accounts for efficient energy usage by the UAV can also be an interesting direction of future research.

**Acknowledgements** This work was supported in part by the UK Science and Technology Facilities Council (STFC) under the Grant No. ST/V00137X/1 and in part by Royal Society under the Grant No. IEC\NSFC\191320.

**Data availability** The data that support the findings of this study are available from the corresponding author upon reasonable request.

## Declarations

**Conflict of interest** The authors declare that they have no conflict of interest.


**Open Access** This article is licensed under a Creative Commons Attribution 4.0 International License, which permits use, sharing, adaptation, distribution and reproduction in any medium or format, as long as you give appropriate credit to the original author(s) and the source, provide a link to the Creative Commons licence, and indicate if changes were made. The images or other third party material in this article are included in the article's Creative Commons licence, unless indicated otherwise in a credit line to the material. If material is not included in the article's Creative Commons licence and your intended use is not permitted by statutory regulation or exceeds the permitted use, you will need to obtain permission directly from the copyright holder. To view a copy of this licence, visit <http://creativecommons.org/licenses/by/4.0/>.

## References

- Ahmad, F., Qiu, B., Dong, X., Ma, J., Huang, X., Ahmed, S., & Ali Chandio, F. (2020). Effect of operational parameters of UAV sprayer on spray deposition pattern in target and off-target zones during outer field weed control application. *Computers and Electronics in Agriculture*, 172, 105350. <https://doi.org/10.1016/j.compag.2020.105350>
- Azizpanah, A., Rajabipour, A., Alimardani, R., Kheiralipour, K., & Mohammadi, V. (2015). Precision spray modeling using image processing and artificial neural network. *Agricultural Engineering International: the CIGR Journal*, 17, 1–10.
- Chen, P., Ouyang, F., Wang, G., Qi, H., Xu, W., Yang, W., Zhang, Y., & Lan, Y. (2021). Droplet distributions in cotton harvest aid applications vary with the interactions among the unmanned aerial vehicle spraying parameters. *Industrial Crops and Products*, 163, 113324. <https://doi.org/10.1016/j.indcrop.2021.113324>
- Choset, H. (2000). Coverage of known spaces: the boustrophedon cellular decomposition. *Autonomous Robots*, 9(3), 247–253. <https://doi.org/10.1023/A:1008958800904>
- Conner, D. C., Greenfield, A., Atkar, P. N., Rizzi, A. A., & Choset, H. (2005). Paint deposition modeling for trajectory planning on automotive surfaces. *IEEE Transactions on Automation Science and Engineering*, 2(4), 381–392. <https://doi.org/10.1109/TASE.2005.851631>
- Coombes, M., Newton, S., Knowles, J., & Garmory, A. (2022). The influence of rotor downwash on spray distribution under a quadrotor unmanned aerial system. *Computers and Electronics in Agriculture*, 196, 106807. <https://doi.org/10.1016/j.compag.2022.106807>
- El Aissaoui, A. (2015). *A feasibility study of direct injection spraying technology for small scale farms: Modeling and design of a process control system*. Université de Liège.

- Fornasiero, D., Mori, N., Tirello, P., Pozzebon, A., Duso, C., Tescari, E., Bradascio, R., & Otto, S. (2017). Effect of spray drift reduction techniques on pests and predatory mites in orchards and vineyards. *Crop Protection*, 98, 283–292. <https://doi.org/10.1016/j.cropro.2017.04.010>
- Forney, S. H., Luck, J. D., Kocher, M. F., & Pitla, S. K. (2017). Laboratory and full boom-based investigation of nozzle setup error effects on flow, pressure, and spray pattern distribution. *Applied Engineering in Agriculture*, 33(5), 641–653.
- Gao, P., Zhang, Y., Zhang, L., Noguchi, R., & Ahamed, T. (2019). Development of a recognition system for spraying areas from unmanned aerial vehicles using a machine learning approach. *Sensors*. <https://doi.org/10.3390/s19020313>
- Guo, S., Li, J., Yao, W., Hu, X., Wei, X., Long, B., Wu, H., & Li, H. (2021a). Optimization of the factors affecting droplet deposition in rice fields by rotary unmanned aerial vehicles (UAVs). *Precision Agriculture*, 22(6), 1918–1935.
- Guo, Y., Liu, C., & Coombes, M. (2021b). Spraying coverage path planning for agriculture unmanned aerial vehicles. *2021 26th International Conference on Automation and Computing (ICAC)*. <https://doi.org/10.23919/ICAC50006.2021.9594271>
- Kamilaris, A., Kartakoullis, A., & Prenafeta-Boldú, F. X. (2017). A review on the practice of big data analysis in agriculture. *Computers and Electronics in Agriculture*, 143, 23–37. <https://doi.org/10.1016/j.compag.2017.09.037>
- Lan, Y., Shengde, C., & Fritz, B. K. (2017). Current status and future trends of precision agricultural aviation technologies. *International Journal of Agricultural and Biological Engineering*, 10(3), 1–17.
- LeCun, Y., Bengio, Y., & Hinton, G. (2015). Deep learning. *Nature*, 521(7553), 436–444.
- Luo, H., Niu, Y., Zhu, M., Hu, X., & Ma, H. (2017). Optimization of pesticide spraying tasks via multi-uavs using genetic algorithm. *Mathematical Problems in Engineering*, 2017, 1–16.
- Meng, Y., Song, J., Lan, Y., Mei, G., Liang, Z., & Han, Y. (2019). Harvest aids efficacy applied by unmanned aerial vehicles on cotton crop. *Industrial Crops and Products*, 140, 111645. <https://doi.org/10.1016/j.indcrop.2019.111645>
- Meng, Y., Su, J., Song, J., Chen, W. H., & Lan, Y. (2020). Experimental evaluation of UAV spraying for peach trees of different shapes: Effects of operational parameters on droplet distribution. *Computers and Electronics in Agriculture*, 170, 105282. <https://doi.org/10.1016/j.compag.2020.105282>
- Mogili, U. M. R., & Deepak, B. B. V. L. (2018). Review on application of drone systems in precision agriculture. *Procedia Computer Science*, 133, 502–509. <https://doi.org/10.1016/j.procs.2018.07.063>
- Mulla, D. J. (2013). Twenty five years of remote sensing in precision agriculture: Key advances and remaining knowledge gaps. *Biosystems Engineering*, 114(4), 358–371. <https://doi.org/10.1016/j.biosystemseng.2012.08.009>
- Qin, W. C., Qiu, B. J., Xue, X. Y., Chen, C., Xu, Z. F., & Zhou, Q. Q. (2016). Droplet deposition and control effect of insecticides sprayed with an unmanned aerial vehicle against plant hoppers. *Crop Protection*, 85, 79–88. <https://doi.org/10.1016/j.cropro.2016.03.018>
- Radoglou-Grammatikis, P., Sarigiannidis, P., Lagkas, T., & Moscholios, I. (2020). A compilation of UAV applications for precision agriculture. *Computer Networks*, 172, 107148. <https://doi.org/10.1016/j.comnet.2020.107148>
- Shilin, W., Jianli, S., Xiongkui, H., Le, S., Xiaonan, W., Changling, W., Zhichong, W., & Yun, L. (2017). Performances evaluation of four typical unmanned aerial vehicles used for pesticide application in China. *International Journal of Agricultural and Biological Engineering*, 10(4), 22–31.
- Tellaache, A., BurgosArtizzu, X. P., Pajares, G., Ribeiro, A., & Fernández-Quintanilla, C. (2008). A new vision-based approach to differential spraying in precision agriculture. *Computers and Electronics in Agriculture*, 60(2), 144–155. <https://doi.org/10.1016/j.compag.2007.07.008>
- Wang, C., He, X., Wang, X., Wang, Z., Wang, S., Li, L., Bonds, J., Herbst, A., & Wang, Z. (2018). Testing method and distribution characteristics of spatial pesticide spraying deposition quality balance for unmanned aerial vehicle. *International Journal of Agricultural and Biological Engineering*, 11(2), 18–26.
- Wang, G., Han, Y., Li, X., Andaloro, J., Chen, P., Hoffmann, W. C., Han, X., Chen, S., & Lan, Y. (2020). Field evaluation of spray drift and environmental impact using an agricultural unmanned aerial vehicle (UAV) sprayer. *Science of the Total Environment*, 737, 139793. <https://doi.org/10.1016/j.scitotenv.2020.139793>
- Zhang, Y., Li, Y., He, Y., Liu, F., Cen, H., & Fang, H. (2018). Near ground platform development to simulate UAV aerial spraying and its spraying test under different conditions. *Computers and Electronics in Agriculture*, 148, 8–18. <https://doi.org/10.1016/j.compag.2017.08.004>

## Authors and Affiliations

Rohit V. Nanavati<sup>1</sup> · Yanhua Meng<sup>2</sup> · Matthew Coombes<sup>1</sup>  · Cunjia Liu<sup>1</sup>

<sup>1</sup> Department of Aeronautical and Automotive Engineering, Loughborough University, Loughborough LE11 3TU, UK

<sup>2</sup> Anyang Institute of Technology, Henan Province 45500, China